Neutron production from thick targets bombarded by alpha particles: Experiment and theoretical analysis of neutron energy spectra

P. K. Sarkar, T. Bandyopadhyay, and G. Muthukrishnan

Health Physics Unit, Variable Energy Cyclotron Centre, Bhabha Atomic Research Centre,
1/AF Bidhan Nagar, Calcutta 700 064, India

Sudip Ghosh

Saha Institute of Nuclear Physics, 1/AF Bidhan Nagar, Calcutta 700 064, India
(Received 5 March 1990)

The neutron energy spectra and angular distributions have been measured for thick targets of ^{9}Be, ^{181}Ta, and ^{197}Au bombarded by 40–60 MeV alpha particles. These data as well as those of other authors have been analyzed in terms of the extended exciton model formalism of nuclear reactions. The model takes into account the emission of neutrons through the single-step direct, multistep direct, multistep compound, and compound-nuclear evaporation processes.

I. INTRODUCTION

Medium-energy ($\sim 10-50$ MeV/nucleon) accelerators are being increasingly used for studies in such diverse fields as material damage studies, production of intense neutron sources, radiation therapy, etc. For these studies, a knowledge of the spectral distribution of neutrons emitted as a result of accelerated charged particles striking a thick target (where the projectile is totally stopped) is important. Most of the work on neutron production from the irradiation of thick targets by charged particles has been done with proton projectiles over a wide energy range.[1] There are also published results of thick-target neutron yield using deuterons, particularly on berrylium and lithium targets which are used as neutron sources for radiation therapy.[1] In contrast, neutron spectra from thick targets and alpha projectiles have been sparsely reported for alpha energies in the range of tens of MeV. The earliest measurements in this energy range were made by Wadman[2] for 40 and 80 MeV alpha on ^{181}Ta. Other measurements have been reported by various authors[3] mostly for alpha energies below 15 and above 500 MeV. More recently, Shin et al.[4] have reported neutron yield distributions from thick targets of carbon, iron, copper, and lead bombarded by 65 MeV alphas. In this paper we report the neutron energy distribution at various angles obtained by bombarding thick targets of ^{9}Be, ^{181}Ta, and ^{197}Au with alpha projectiles at incident energies of 40 (for ^{197}Au), 50 (for ^{9}Be and ^{181}Ta), and 60 MeV (for ^{181}Ta).

In addition to the paucity of data on neutron yields from thick targets irradiated with alphas, the reaction mechanisms for neutron emission from thick targets are not well understood. From the point of view of studying nuclear reactions, thick targets have an advantage over thin targets in the sense that measurements at extreme forward angles are possible and these data are expected to explain the role of direct reaction processes. However, unlike the case of thin targets where the reaction takes place at a given projectile energy, the measured spectrum from thick targets is a superposition of spectra corresponding to projectile energies continuously decreasing from its initial value to the threshold for neutron production. Nevertheless, if depletion of projectile energy inside the target is taken into account, a proper theoretical analysis is expected to give some understanding of the reaction mechanisms involved.

The data on neutron yield from various thick-target–projectile combinations have mostly been analyzed in terms of Monte Carlo calculations of the intranuclear cascade (INC) and evaporation models. These calculations, however, are constrained by the lower limit set on the projectile energy. For instance, Nakamura et al.[5] and Shin et al.[4] had obtained the neutron yield data from the bombardment of thick targets of C, Fe, Cu, and Pb by 30 and 50 MeV protons, 33 MeV deuterons, and 65 MeV ^{3}He and alphas. They used Bertini's code MECC-7 of the INC and evaporation models for the analysis of the 50 MeV proton data alone since this code is valid for projectile energies greater than 50 MeV/nucleon. Lower projectile energies of 16.1 MeV/nucleon for deuterons, 17.6 MeV/nucleon for ^{3}He, and 22.1 MeV/nucleon for alphas can be treated by the LHI (light heavy ion) code which uses the same INC and evaporation model of MECC-7. But even this code could be used only for the 33 MeV deuteron and 65 MeV ^{3}He data of Ref. 4 and not for the 65 MeV alpha since the projectile energy in the last case is well below the lower limit for alpha projectile (22.1 MeV/nucleon) in the LHI code.

To avoid this constraint of Monte Carlo calculations, Nakamura and Uwamino[6] invoked the well-known preequilibrium and compound-nuclear emission mechanisms of nuclear reactions to phenomenologically analyze the neutron yield data from thick targets. They made the common assumption that both the preequilibrium and evaporation spectra can be described by Maxwellian-type functions with different "temperatures" or slope parame-

ters of the logarthimic yield as a function of neutron energies and emission angles. From a systematic study of the experimental data, Nakamura and Uwamino obtained an empirical expression for the "temperature" for the compound-nuclear emissions.
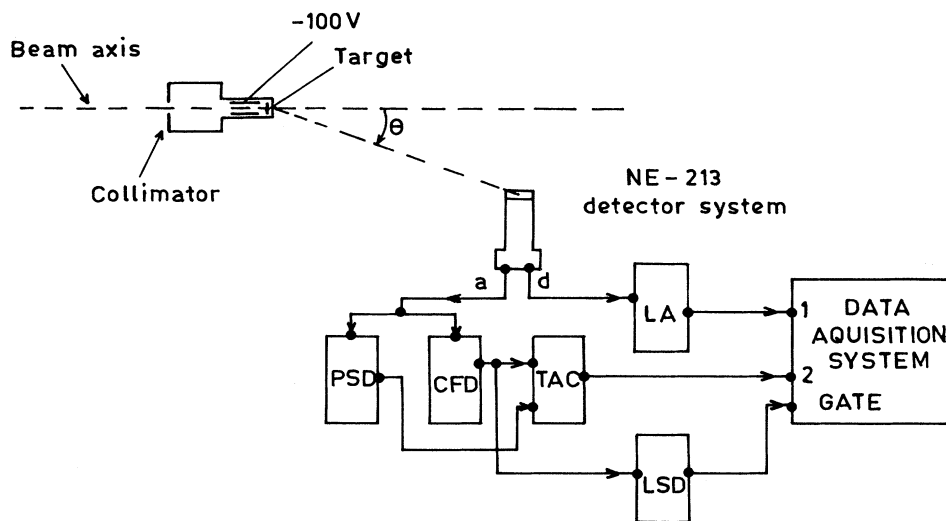
It was observed by these authors that the "temperature" for the compound-nuclear evaporation shows a dependence on the neutron emission angle for low-mass target nuclei, but this angle dependence vanishes with heavier targets. In the case of the preequilibrium component, however, the "temperature" is dependent on the emission angle for both light and heavy targets. It was found to decrease with increasing emission angle but otherwise no systematic trend could be discerned in the behavior of the preequilibrium "temperature" to obtain even an empirical relation.

For a better understanding of the reaction mechanism for the emission of neutrons from thick targets, we have used here the well-known exciton model for preequilibrium emissions and the Weisskopf-Ewing calculations for compound-nuclear evaporations. There are various versions of the exciton model, all of which can explain the angle-integrated preequilibrium ejectile spectra quite satisfactorily. These models, however, fail to account for the observed angular distributions in preequilibrium emissions, particularly at backward angles where the models underpredict the cross section by as much as an order of magnitude. In order to remove these discrepancies, Kalbach and Mann[7] (KM) made a systematic study of a large number of angular distribution data from reactions induced by proton, deutron, ^{3}He, and alpha projectiles and found that the observed angular distributions can be described in terms of Legendre polynomials whose coefficients are given by simple phenomenological relations. A good fit of the calculated angular distribution from the KM parametrization with the exclusive angular distribution of neutrons from $(\alpha, xn\gamma)$ reactions on thin targets has been reported by Fields et al.[8] In the present work we use the same formalism to study our inclusive neutron spectra from thick targets. For this purpose we have modified Kalbach's code PRECO-D2,[9] which incorporates the above formalism, to calculate thick-target neutron yield.

II. EXPERIMENTAL PROCEDURE

The experimental arrangement is shown in Fig. 1. Accelerated alpha particles of different energies from the cyclotron at the Variable Energy Cyclotron Centre, Calcutta, bombarded thick targets of ^{9}Be, ^{181}Ta, and ^{197}Au. The beam energy resolution was about 200 keV for 40–60 MeV incident alphas. The projectile energies, the targets used, and their thicknesses are shown in Table I. The targets (25 mm in diameter) were fixed perpendicularly to the beam axis. The thicknesses of the targets are such that the incident alphas are completely stopped in the target while the scattering and absorption of neutrons produced in the target are negligible. The neutrons emit-

a : Anode
d : Dynode
LA : Linear amplifier
PSD : Pulse shape discriminator
CFD : Constant fraction discriminator
TAC : Time to amplitude converter
LSD : Logic shaper and delay

FIG. 1. Schematic diagram of experimental arrangement with associated electronics.

TABLE I. List of targets, projectile energies, and target thicknesses.

Target	Energy (MeV)	Thickness (mm)
^{9}Be	50	3.0±0.05
^{181}Ta	50,60	4.0±0.05
^{197}Au	40	0.8±0.05

ted at 0°, 30°, 60°, and 90° with respect to the incident beam were measured with a 52.4 mm $\phi \times 52.4$ mm NE-213 liquid scintillator kept at a distance of 1.4 m from the target. The detector angle of acceptance was 2.14° and energy resolution was ~20%.

A collimator at a distance of 20 cm in from of the target was used to restrict the beam size to about 10 mm. The collimator was electrically insulated from the target as well as the beam tube. The beam current was minimized on the collimator and maximized on the target. The beam falling of the collimator was always kept below 0.5% of the beam on the target, thus reducing the background neutron contribution to negligible proportions. The number of particles incident on the target was measured by the current integrator connected to the target. The target was surrounded by a suppressor grid (-100 V). Beam currents used for the present work are of the order of 100 nA except in the case of the Be target where about 20 nA of beam current was used. The maximum uncertainty in beam-current measurement was estimated to be 5%.

In order to estimate the background contribution from the room-scattered neutrons, a shadow bar was interposed between the detector and the target. The prespex shadow bar of length 100 cm and diameter 10 cm stops the direct contribution of the neutrons produced from the target. Measurements taken with the interposed shadow bar give the room-scattered component which was subtracted from the original spectrum. It was observed that the background neutrons contribute between 5 and 10% to the neutrons measured without the shadow bar. The spectra reported are corrected for this scattered component. An example of the raw neutron yield data with and without the shadow bar is shown in Fig. 2.

The light output pulse and the corresponding rise time of the pulse was collected in a two-parameter mode using a high-speed data-acquisition system based on computer automated management and control (CAMAC) for Norsk Data ND-560 computer. The hardware and software details of the system are given in Ref. 10. The pulse from the anode of the photomultiplier was analyzed for its shape and then fed to a time-to-amplitude converter (TAC). The output of the TAC serves as input for one parameter which gives the rise-time distribution of the pulses. The pulse from the last dynode of the photomultiplier after proper amplification and delay is the input for the other parameter which gives information on the energy distribution of the pulses. An off-line discrimination of the neutron and gamma pulses was carried out from the two-dimensional display of the data and a properly constructed banana gate. This method enables accurate discrimination of neutron and gamma pulses based

on their difference in rise-time distributions over a wide dynamic range. The energy calibration of the system was done by ^{137}Cs (0.66 MeV) and ^{22}Na (0.51 and 1.2 MeV) gamma rays.

The pulse-height output distributions were unfolded to obtain neutron energy spectra with the revised FERDO unfolding code using the Monte Carlo calculated response functions.[11] The errors associated with the unfolded distributions are (i) the statistical error associated with the measurement, (ii) the error arising from the discretization of a continuous spectrum and response function, and (iii) the statistical error inherent in the Monte Carlo calculation of the response matrix.

The statistical error associated with the measurement is low for high neutron yield (low-energy neutrons) and higher when the neutron yield is low (higher neutron energies). For low-energy neutrons, this contributes ~5–10% of the total error, while for higher-energy neutrons this contributes ~15–20% of the total error. The discretization error is less than 1% of the total error and does not change appreciably with neutron energy. The maximum contribution to the error comes from the statistical uncertainty associated with the calculated response functions. At low energies this constitutes 85–95% and at high energies 75–85% of the total error. The total error varies from about 2 to 5% of the yield at high neutron yields ($\sim 10^{-5}$ neutrons MeV^{-1} sr^{-1} alpha^{-1}) to about 80% at very low yields ($\sim 10^{-9}$ neutrons MeV^{-1} sr^{-1} alpha^{-1}). All these errors are included in the error bars in Figs. 2–7.

III. RESULTS AND COMPARISON WITH REACTION MODEL

A. Experimental results

In Figs. 3–6 are plotted the neutron energy spectra $\phi(\varepsilon,\theta)$ with the corresponding errors for 50 MeV alphas on ^{9}Be, 50 and 60 MeV alphas on ^{181}Ta, and 40 MeV alphas on ^{197}Au at emission angle of $\theta=0°$, 30°, 60°, and 90°. The data given are normalized to one incident alpha particle on each target.

The following observations can be made from the neutron spectra in these figures.

(1) Two components exist in the measured distributions from ^{181}Ta and ^{197}Au, one below 10 MeV corresponding to evaporation neutrons and the other above 10 MeV due to the neutrons from the preequilibrium processes. The preequilibrium component decreases with increasing angle as expected.

(2) A shoulder or bump is observed in the energy spectra at lower emission angles. This starts around 10 MeV for 50 and 60 MeV alphas on ^{181}Ta at emission angle 0°. A similar but less prominent bump can be observed for 40 MeV alphas on ^{197}Au at emission angle 0° and for 60 MeV alphas on ^{181}Ta at emission angle 30°. The occurrence of this bump at 0° for 40 and 50 MeV projectiles and its absence at higher angles indicates that it results from direct reaction processes.

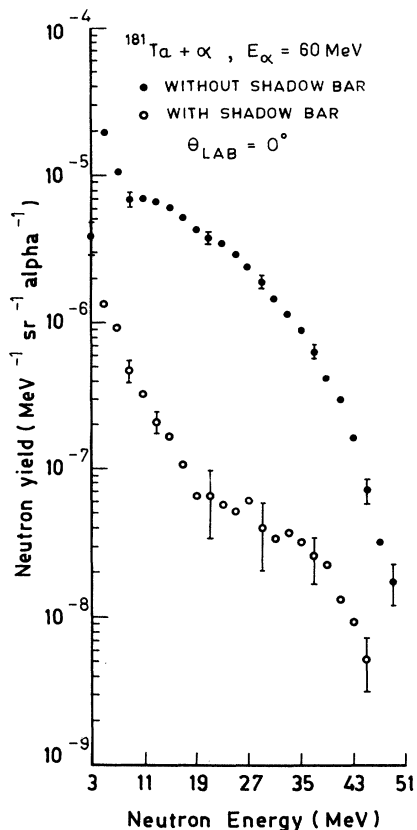(3) Neutron spectra from 50 MeV alphas on ^{9}Be do not match in shape with the spectra from other targets.

FIG. 2. Example of the raw neutron spectra obtained with (O) and without (●) shadow bar for ^{181}Ta target and 60 MeV incident alpha at 0° laboratory angle.

There is, however, a low-energy component, arising presumably from evaporation neutrons, and also a high-energy component decreasing with increasing angle and therefore presumed to be the preequilibrium component. In addition, there is a third component occurring in between the two in the neutron energy region from 10 to 25 MeV at all emission angles. In this region the neutron yield remains more or less constant with respect to emission energy. A multibody breakup of ^{9}Be through α bombardment rather than the well-known neutron emission through the formation of a ^{12}C residual nucleus may be responsible for this component of the spectrum.

B. Theoretical calculations

For the theoretical analysis of the preequilibrium component of the measured spectrum, we have used the exciton model formalism of Griffin as extended by Kalbach[12] to include contributions from the statistical multistep direct (MSD) and the statistical multistep compound (MSC) processes of the Feshbach-Kerman-Koonin quantum-mechanical theory[13] of preequilibrium nuclear reactions. In the MSD process, at least one of the excited particles is in the continuum at each stage of the relaxation process, while in the case of MSC emissions all excited particles are bound and emissions take place through statistical fluctuations. The ejectile angular distributions are forward peaked in the MSD emissions and in the case of MSC they are symmetric about the 90° center-of-mass angle.

In the exciton model, the target-projectile composite nucleus is assumed to reach compound nucleus equilibrium through a cascade of two-body interactions. Each
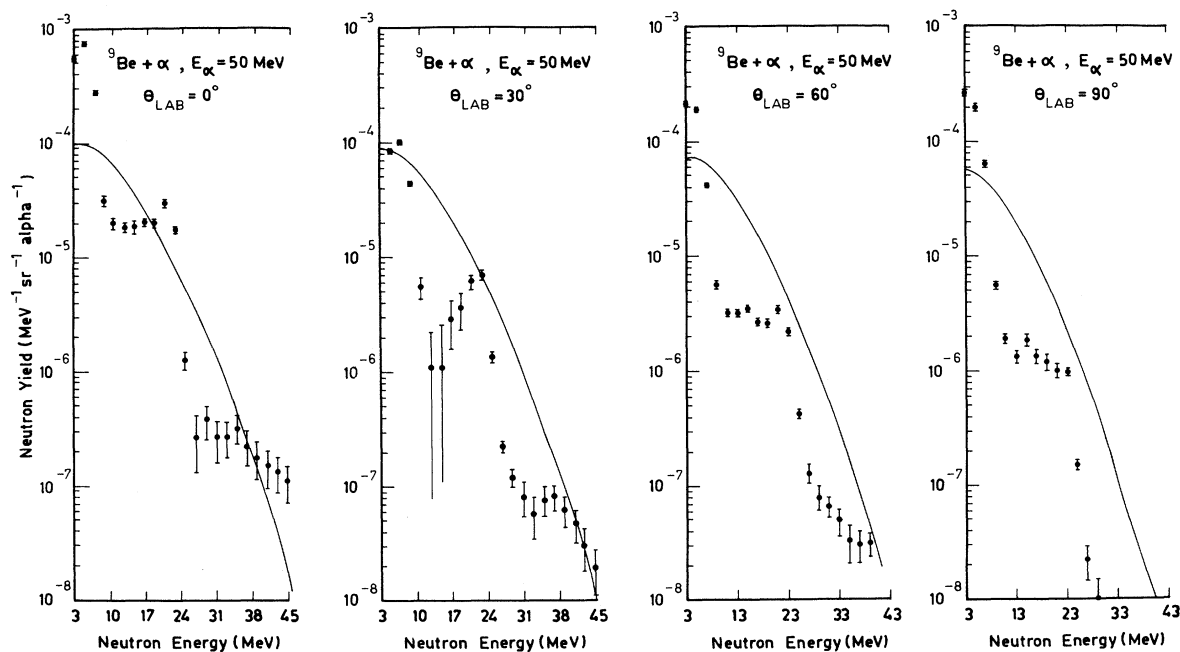

FIG. 3. Neutron spectra from ^{9}Be target with 50 MeV alpha at 0°, 30°, 60°, and 90° emission angles. Experimental data are plotted in solid circles with error bars and the solid lines are the theoretical calculations of the extended exciton model of Kalbach (Ref. 12).
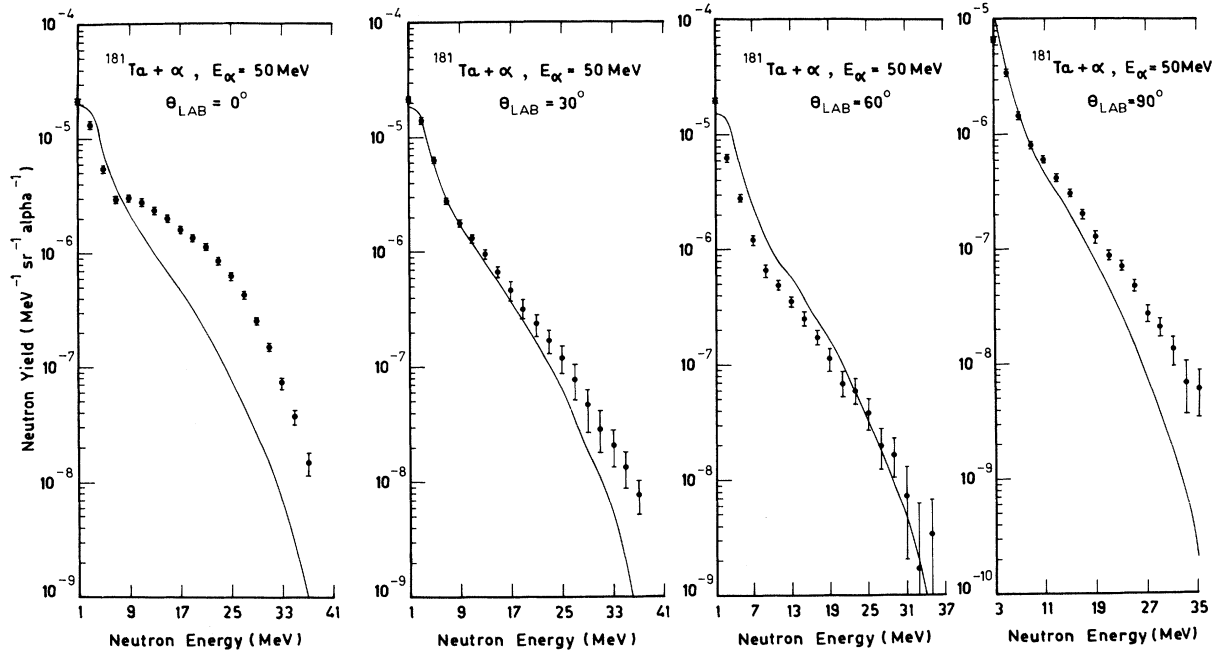
FIG. 4. Same as Fig. 3 for ^{181}Ta target and 50 MeV incident alpha.

stage of the binary cascade is characterized by the number of excited particles (p) and holes (h) termed as excitons. Emissions can take place from any stage of the binary cascade.

The total preequilibrium differential cross section $\sigma_{\text{pre}}(E_a;\varepsilon)$ is the sum of the MSD and MSC components $\sigma_{\text{MSD}}(E_a;\varepsilon)$, respectively,

$$\sigma_{\text{pre}}(E_a;\varepsilon)=\sigma_{\text{MSD}}(E_a;\varepsilon)+\sigma_{\text{MSC}}(E_a;\varepsilon) , \tag{1}$$

where E_α and ε are the projectile and ejectile energies, respectively. Kalbach[12] evaluates the MSD component from the relation

$$\sigma_{\text{MSD}}(E_a,\varepsilon)=\sigma_{\text{abs}} \sum_{p=p_0}^{\bar{p}} S_d(p,h)T_u(p,h)\lambda_b^u(p,h,\varepsilon) , \tag{2}$$

where σ_{abs} is the absorption cross section of the projectile by the target, p_0 is the number of particles excited at the
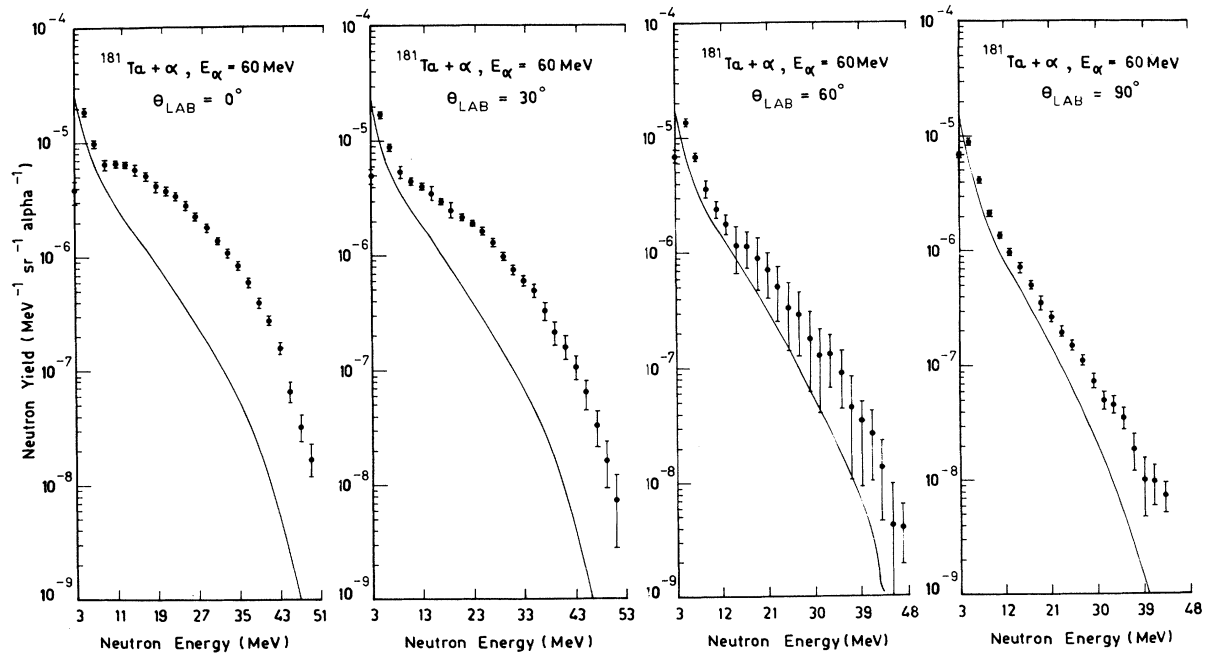

FIG. 5. Same as Fig. 3 for ^{181}Ta target and 60 MeV incident alpha.

first stage of the binary cascade, and $\bar{p}$ is the number of excited particles in the equilibrated compound nucleus. The summation over p ensures contributions from all stages of the cascade. $S_d(p,h)$ is the probability of the formation of the (p,h) configuration with at least one unbound particle from earlier configurations which all had at least one particle in the continuum. $T_u(p,h)$ is the mean lifetime of the (p,h) configuration and $\lambda_b^u(p,h,\varepsilon)$ is the emission rate of the b-type particle with energy ε from the (p,h) configuration. Kalbach[12] calculates $S_d(p,h)$ and $T_u(p,h)$ by separately evaluating the phase-space available to the bound and unbound excited particles in each (p,h) configuration.

The total preequilibrium cross section $\sigma_{\mathrm{pre}}(E_a;\varepsilon)$ is evaluated using the standard Griffin exciton model and the MSC component is obtained as

$$\sigma_{\mathrm{MSC}}(E_a;\varepsilon)=\sigma_{\mathrm{pre}}(E_a;\varepsilon)-\sigma_{\mathrm{MSD}}(E_a;\varepsilon) . \tag{3}$$

Also included in the Kalbach formalism are two classes of direct reactions which are not taken into account in the calculation of the MSD component from Eq. (2). These are the nucleon transfer and nucleon knockout reactions. These are evaluated semiempirically. The nucleon transfer cross section $\sigma_N(E_a;\varepsilon)$ is obtained from

$$\sigma_N(E_a;\varepsilon)=0.0127\frac{(2S_b+1)A_b\varepsilon\sigma_{\mathrm{inv}}^b(\varepsilon)}{(2S_a+1)A_a^2\varepsilon_a}$$

$$\times K_{\alpha,p}\left[\frac{A_a}{E_a+V_a}\right]^{2n}\left[\frac{2860}{A_R}\right]^n$$

$$\times\left[\frac{2Z_T}{A_T}\right]^{6n_\pi}\frac{p!h!}{p_\pi!p_\nu!h_\pi!h_\nu!}$$

$$\times\frac{g_\pi^{n_\pi}g_\nu^{n_\nu}}{g^n}\omega(p,h,U) , \tag{4}$$

where S_a and S_b are the intrinsic spins of the projectile and the ejectile, respectively, and A_a and A_b are mass numbers. $\sigma_{\mathrm{inv}}^b(\varepsilon)$ is the inverse cross section. Z_T and A_T are the charge and mass numbers of the target and A_R is the mass number of the residual nucleus. The quantities E_a and ε_a are the laboratory and center-of-mass energies of the projectile and V_a is the average potential seen by the projectile in the direct reaction region. It is taken to

be one-fourth of the real central well depth: $V_a=50A_a/4$ MeV. p_π and p_ν are the number of stripped protons and neutrons and h_π and h_ν are the number of picked-up protons and neutrons $p=p_\pi+p_\nu$, $h=h_\pi+h_\nu$, $n_\pi=p_\pi+h_\pi$, $n_\nu=p_\nu+h_\nu$. The constant $K_{\alpha,p}$ gives a factor of 12 enhancement to the nucleon transfer whenever the projectile and the ejectile are both tightly bound; i.e., a nucleon or an alpha particle. It is unity for all other cases. g_π and g_ν are the single-particle level densities for protons and neutrons in the residual nucleus and are given by $g_\pi=(Z_R/A_R)g_R$, $g_\nu=(N_R/A_R)g_R$, where Z_R and N_R are the residual charge and neutron numbers and g_R is the total single-particle level density $(g_R=g_\pi+g_\nu)$ of the residual. $\omega(p,h,U)$ is the particle state density of the residual nucleus in the (p,h) configuration and excitation U. It is of the form[14]

$$\omega(p,h,U)=\frac{g_R^{p+h}(U-A_{p,h})^{p+h-1}}{p!h!(p+h-1)!} ,$$

$$A_{p,h}=\frac{p_m^2}{g_R}-\frac{p^2+h^2+p+h}{4g_R} , \tag{5}$$

where $A_{p,h}$ is the Pauli correction to the partial level density with $p_m=\max(p,h)$.

The origins of the various factors in the semiempirical expression (4) and their validity are discussed in Ref. 14. For instance, the transfer of n number of nucleons will be more probable the longer the time spent by the projectile in the direct reaction region. This is taken care of by the factor $[A_a/(E_a+V_a)]^{2n}$; E_a+V_a, being the projectile energy in the region of direct reaction, is proportional to the square of the velocity. The theoretical work of Iwasaki[15] shows the single nucleon transfer probability to be inversely proportional to the mass number and expects the transfer probability of n nucleons to vary as the power n of the probability. This is taken care of by the factor $(2860/A_R)^n$. The proton and neutron transfer probabilities are expected to depend on the proton and neutron richness of the target nucleus and this is accounted for through the factor $(2Z_T/A_T)^{6n_\pi}$.

In evaluating the knockout reaction component, Kalbach assumes the single-step knockout process in competition with the single-step inelastic scattering of the projectile and uses the following semiempirical equation to calculate the knockout cross section:

$$\sigma_{\mathrm{KO}}(E_a;\varepsilon)=(\sigma_{\mathrm{abs}}/13.5)(2S_b+1)A_b\varepsilon\sigma_{\mathrm{inv}}^b(\varepsilon)\frac{P_bg_ag_b(U-A_{A_a,A_b})}{\displaystyle\sum_{c=a,b}(2S_c+1)A_c\bar{\sigma}_{\mathrm{inv}}^c(\varepsilon_m+2B_c)(\varepsilon_m-B_c)^2(g_ag_b^2/6g_c)} . \tag{6}$$

P_b is the probability of exciting a b-type particle-hole pair through the first two-body interaction. In the present case b is a neutron and P_b is assumed by Kalbach to be the ratio N_T/A_T. A_{A_a,A_b} is the Pauli correction as in (5) with A_a and A_b replacing p and h, respectively. ε_m is the energy of the ground-state transition of a particle of type c. $\bar{\sigma}_{\mathrm{inv}}^c$ is the inverse cross section averaged over all

emission energies. g_a and g_b are the single-particle level densities of the projectile and ejectile, respectively, and A_a and A_b are the mass number of the projectile and the ejectile respectively. B_c is the separation energy of c-type particles.

The neutron angular distributions are evaluated from the KM systematics.[7] Kalbach and Mann break

up the preequilibrium angular distribution into two components—the MSD and MSC with the nucleon transfer and knockout components included in MSD and the Weisskopf-Ewing compound-nuclear component $\sigma_{\text{evap}}(E_a, \varepsilon)$ included in the MSC. For a given projectile energy E_a, the double-differential cross section is

$$\sigma(E_a; \varepsilon, \theta) = a_0(\text{MSD}) \sum_{l=0}^{l_{\max}} b_l P_l(\cos\theta)$$

$$+ a_0(\text{MSC}) \sum_{l=0}^{l_{\max}} b_l P_l(\cos\theta) \ ,$$

$$a_0(\text{MSD}) = \frac{1}{4\pi} [\sigma_{\text{MSD}}(E_a; \varepsilon) + \sigma_N(E_a; \varepsilon) \tag{7}$$

$$+ \sigma_{\text{KO}}(E_a; \varepsilon)] \ ,$$

$$a_0(\text{MSC}) = \frac{1}{4\pi} [\sigma_{\text{MSC}}(E_a; \varepsilon) + \sigma_{\text{evap}}(E_a; \varepsilon)] \ .$$

The coefficients b_l are functions of the ejectile energy and are assumed to be of the form

$$b_l = \frac{2l+1}{1 + \exp[A_l(B_l - \varepsilon - \mathcal{B})]} \ , \tag{8}$$

$\mathcal{B}$ being the ejectile binding energy. The parameters A_l and B_l are free parameters and have been obtained in the KM systematics by fitting with observed angular distributions as

$$A_l = [0.036 + 0.0039l(l+1)] \ \text{MeV}^{-1} \ ,$$
$$B_l = \left\{ 98 - \frac{90}{[l(l+1)]^{1/2}} \right\} \ \text{MeV}^{-1} \ . \tag{9}$$

C. Calculations for thick-target neutron yield

To calculate the energy and angular distribution of neutrons emitted from a thick target, we divide the target into a number of thin slabs, calculate the spectra from each slab, and sum them to obtain the total emitted spectrum. While considering the continuous slowing down of the projectile, we make the usual assumption[5] of ignoring the multiple scattering and straggling of the projectile as well as the negligible scattering of the emitted neutrons in the target. The thickness of each slab was so selected that the alpha projectile loses ΔE MeV energy in each slab. The kinetic energy by the alpha incident on the ith slab E_a^i and the average energy in the ith slab $\bar{E}_a^i$ are given by

$$E_a^i = E_a^0 - (i-1)\Delta E \ ,$$
$$\bar{E}_a^i = (E_a^i + E_a^{i-1})/2 \ . \tag{10}$$

The slab thickness x_i is

$$x_i = \int_{E_a^i}^{E_a^{i+1}} \frac{dE}{-dE/dx} \ , \tag{11}$$

where dE/dx is the alpha stopping power for the target material as taken from Ref. 16.

The neutron yield $\phi(\varepsilon, \theta)$ at energy ε and direction θ is given by

$$\phi(\varepsilon, \theta) = \sum_{i=1}^{m} \sigma(\bar{E}_a^i; \varepsilon, \theta) N x_i$$

$$\times \exp\left\{ -N \left[\sum_{k=1}^{i-1} \sigma_{\text{abs}}(\bar{E}_a^k) x_k \right] \right\} \ , \tag{12}$$

where N is the target atomic density. $m = (E_a^0 - E_a^{\text{th}})/\Delta E$, E_a^{th} being the projectile threshold energy for neutron production. For $i = 1$, the value of the exponential attenuation factor in (12) is taken to be unity.

The value of $\sigma(\bar{E}_a^i; \varepsilon, \theta)$ and σ_{abs} for alphas of energy $\bar{E}_a^i$ are calculated using Eq. (7) for all $\bar{E}_a^i$, $i = 1, \ldots, m$. We have used the code PRECO-D2 written by Kalbach[9] which incorporates all the features described above. The code has been modified to include calculations involving Eqs. (10)–(12). The single-particle level density g is taken as $A/13$. The code calculates the projectile absorption cross sections σ_{abs} and the inverse reaction cross section σ_{inv} using the empirical approximation of Ref. 17. For the preequilibrium calculations we have assumed that the incident alpha is removed from the entrance channel by a two-body interaction with an individual target nucleon. The initial number of excited particles p_0 and holes h_0 are accordingly chosen as $p_0 = 5$, $h_0 = 1$.

D. Comparison with theoretical calculations

The comparison between the theoretical calculations and the energy spectra at different laboratory angles obtained in the present experiment are shown in Figs. 3–6. For the purpose of understanding the reaction mechanism, we have also included in the comparison the data of Shin et al.[4] from the irradiation of Cu (Fig. 7) by 65 MeV alpha particles. The calculated yield of the Cu target was obtained by evaluating the yields separately for ^{63}Cu and ^{65}Cu and taking the sum in the proportion of their natural abundances. The theoretical calculations are in the center-of-mass frame while the experimental yields are in the laboratory frame. Except in the case of the ^{9}Be target, there will be no significant change in converting from one system to the other due to the low velocity of the center of mass for heavier targets.

It can be seen that, except for ^{9}Be shown in Fig. 3, the calculated energy spectra for all other targets agree well with experiment for larger angles. For the forward angles the high-energy part is always underpredicted, though the low-energy part is satisfactorily explained but less so for the Cu target. Also, for the forward angles, the bump occurring in the intermediate region has not been reproduced—the yields are always underpredicted in these regions.

For the ^{9}Be target the agreement of the theoretical spectra with experiment is poor at all angles. The calculations do not agree either with the absolute values or with the trend. Apart from the differences arising out of measurements in the laboratory frame and calculations in the center of mass, it should be pointed out that the neutron yield was theoretically calculated assuming the reaction to proceed through the formation of the ^{12}C residual
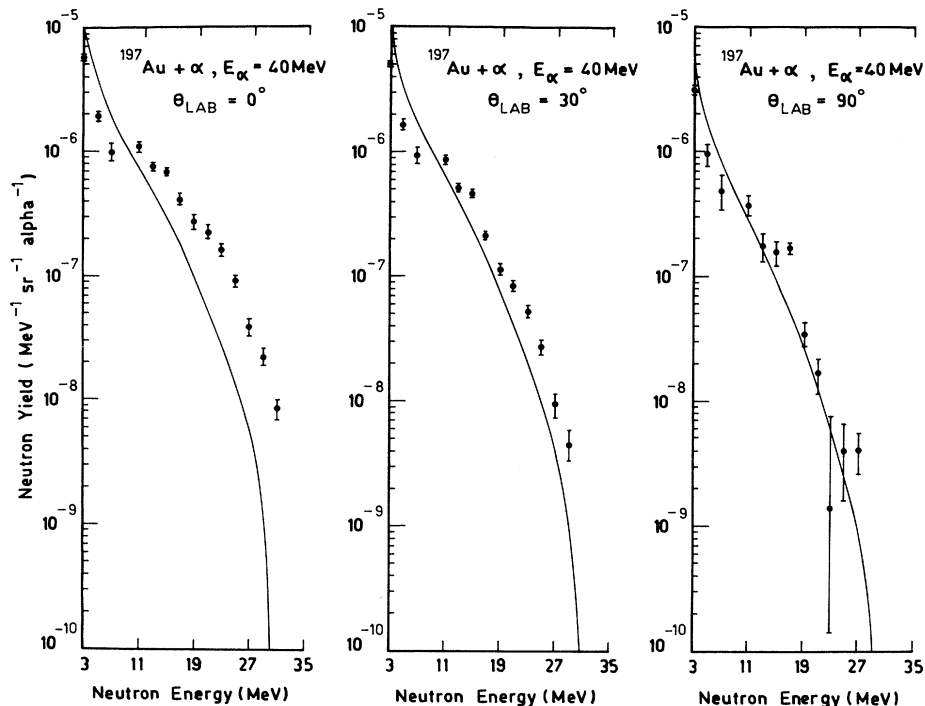
FIG. 6. Same as Fig. 3 for ^{197}Au target and 40 MeV incident alpha.

nucleus. It seems from the observed data between 10 and 25 MeV at all angles that there are significant contributions from the multibody breakup of ^{9}Be which could not be incorporated in the present formalism.

In order to understand the failure of Kalbach's extended exciton model formalism to explain the forward-angle

high-energy component as well as the bumps occuring at intermediate-energy regions, we have compared the calculated and experimental angle integrated spectra in Figs. 8–10. For this purpose we have broken up the calculated yield into its components of knockout, nucleon transfer, MSD, MSC and Weisskopf-Ewing evaporations. The an-
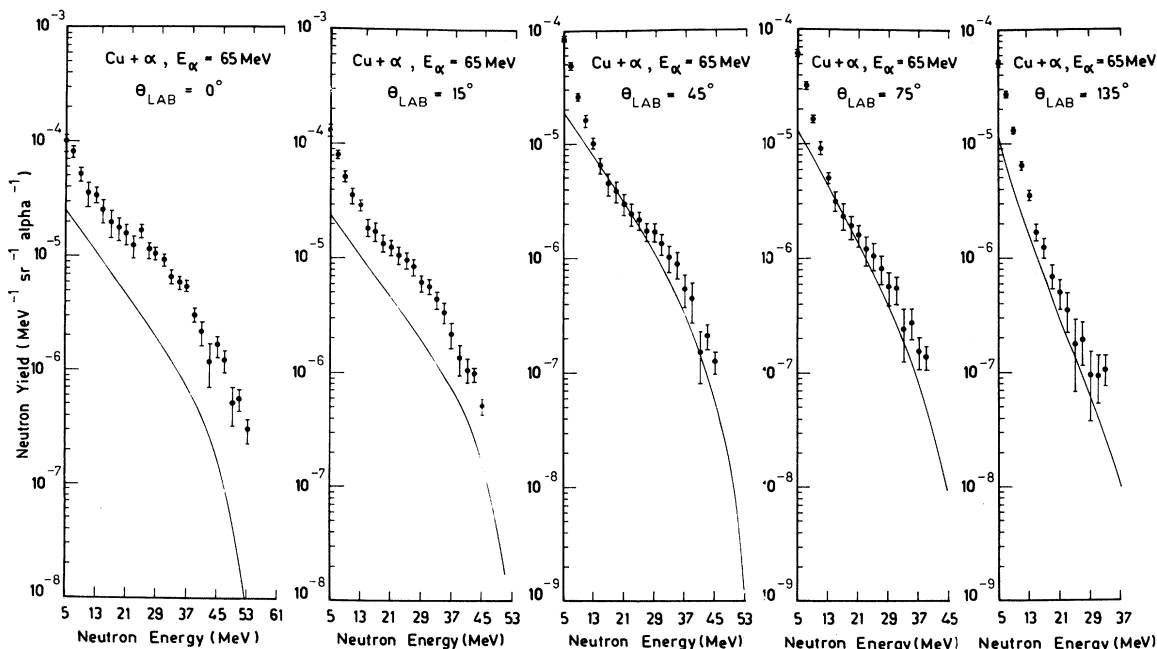

FIG. 7. Shows the comparison of the theoretical calculations of the extended exciton model of Kalbach (Ref. 12) with the experimental neutron spectra from Cu with 65 MeV incident alpha at emission angles of 0°, 15°, 45°, 75°, and 135°. The experimental results are those of Shin et al. (Ref. 4).

gle integration of the experimental data has been per-formed using the trapezoidal rule. Since there are no ex-perimental data for angles larger than 90° for ^{181}Ta and ^{197}Au, the calculated angle-integrated neutron yield and its components were obtained by integrating the theoreti-cal angular distribution up to 90° with the help of (7).

For the targets ^{181}Ta (Fig. 8) and ^{197}Au (Fig. 9), the low-energy component (up to ~5 MeV) is reproduced by the Weisskopf-Ewing evaporation calculations. The MSD component makes significant contributions for neu-tron energies between 5 and 20–25 MeV. The MSC con-tributions are always smaller than the evaporation com-ponent except at higher neutron energies (above 10 for 40–50 MeV projectiles and above 12 MeV for higher-energy projectiles). The high-energy component (beyond 20–25 MeV) of the calculated spectra is made up of the MSD part together with the direct components of nu-clear transfer and knockout. The latter are the dominant components at very high neutron energies. Both the knockout and the neutron transfer are equally important.

For the Cu target (Fig. 10) the contributions from the various components are similar except for two features. First, at low energies the evaporation component is not sufficiently strong to account for the total yield and the MSD component is more important. A possible reason may be that the choice of the single-particle level density $g = A/13$ is not a proper value in this case. As is well known even a small increase in the value of g will result in a substantial enhancement of the evaporation com-ponent. Secondly, the contribution from nucleon transfer [Eq. (4)] is far stronger than that from the knockout com-ponent [Eq. (6)]. In the nucleon transfer reaction com-ponent evaluated from (4), the factor $(2Z_T/A_T)^{6n_\pi}$ is 0.37 and 0.25 for ^{63}Cu and ^{65}Cu, respectively. For ^{181}Ta and ^{197}Au this factor is of the order of 0.075. As a conse-quence, the nucleon transfer component for the Cu target is far stronger.

As can be seen from Figs. 8–10, the failure of calculat-ed yields to account for the high-energy component as
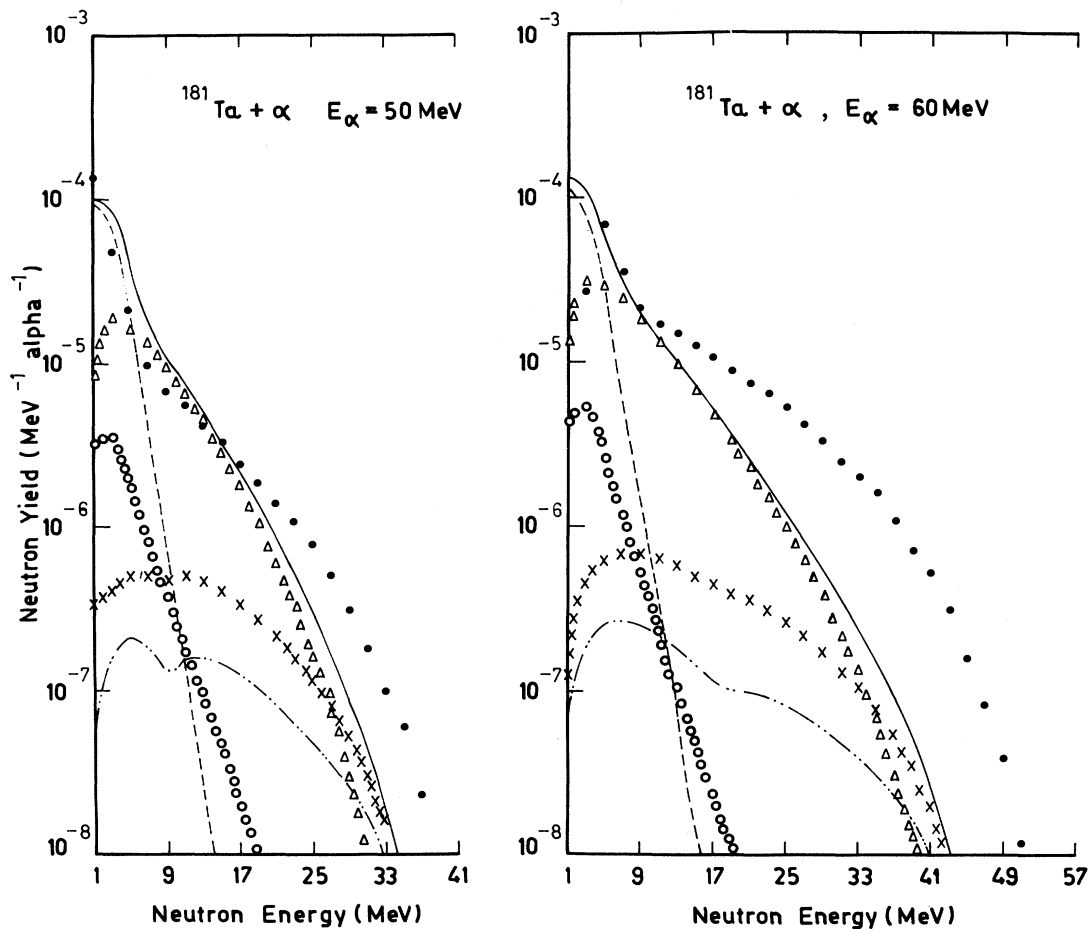

FIG. 8. Comparison of the experimental (●) angle-integrated neutron energy spectra from ^{181}Ta at 50 and 60 MeV incident alpha with calculations (———) of the extended exciton model (Ref. 12). Also shown are the various components of the calculated spectra: evaporation component (— — —), MSD component ($\triangle\triangle\triangle$), MSC component ($\circ\circ\circ$), neutron knockout component (—··—), and the sum of transfer and knockout components ($\times\times\times$).

SARKAR, BANDYOPADHYAY, MUTHUKRISHNAN, AND GHOSH

well as the bump in the intermediate-energy region may be due to the underprediction of the direct components. As has been discussed in Sec. II B, the yields from the direct components of nucleon transfer and knockout have been calculated using the semiempirical equations (4) and (5). The parameters in these expressions have been evaluated by Kalbach[14] by fitting with experimental data of (p,p'), (p,d), (p,t), $(p,{}^{3}\text{He})$, (p,α), (α,α'), (α,p), (α,d), (α,t), and $(\alpha,{}^{3}\text{He})$ on ${}^{54}\text{Fe}$, ${}^{120}\text{Sn}$, and ${}^{197}\text{Au}$ targets. No data on (α,n) reactions have been considered in Ref. 14 to arrive at the values of the various parameters. Some of the parameters can be altered to some extent to enhance the contribution from the direct components. For instance, in the present case of an α projectile and a neutron ejectile, the parameter $K_{\alpha,p}$ in (4) has been assigned a value of 12 by Kalbach. An increase in the value of $K_{\alpha,p}$ would obviously increase the yield linearly. Again, the average potential V_a seen by the projectile in the region of nucleon transfer has been taken to be $50 A_a / 4$. Confining the region of nucleon transfer to a narrower surface region would obviously decrease V_a and thereby increase the yield substantially on account of the exponent $2n$ in the factor $[A_a / (E_a + V_a)]^{2n}$ ($n = 3$ in the present case). However, we have not undertaken any such modification

of the parameters since the data presented in this work are not sufficient to arrive at any globally optimum value.

The MSD component is the dominant process for the neutron yield for energies between 5 and 20–25 MeV. At higher energies it also makes significant contributions together with the knockout and transfer components. It is, therefore, interesting to investigate whether the MSD component can be increased to remove, or at least reduce the observed discrepancies. The MSD component can be altered by changing the initial number of excited particles p_0 and holes h_0. We have assumed that the incident alpha is removed from the entrance channel by interacting with a target nucleon to create a particle-hole pair. The values of p_0 and h_0 were taken to be 5 and 1, respectively. Another way by which the incident alpha can be removed from the entrance channel to form the target+projectile composite nucleus is through its complete dissolution into four nucleons in the nuclear force field.[18] This process is most likely to occur at the nuclear surface. In this case, no particle-hole pair is created and the initial exciton numbers are $p_0 = 4$ and $h_0 = 0$. That this choice of p_0, h_0 values does appreciably increase the MSD component is shown in Fig. 11 where the MSD components of the neutron yield from ${}^{181}\text{Ta}$ at 50 MeV incident alpha energy have been compared for $p_0, h_0 = 5, 1$ and $p_0, h_0 = 4, 0$. Figure 12 shows a comparison of the angu-
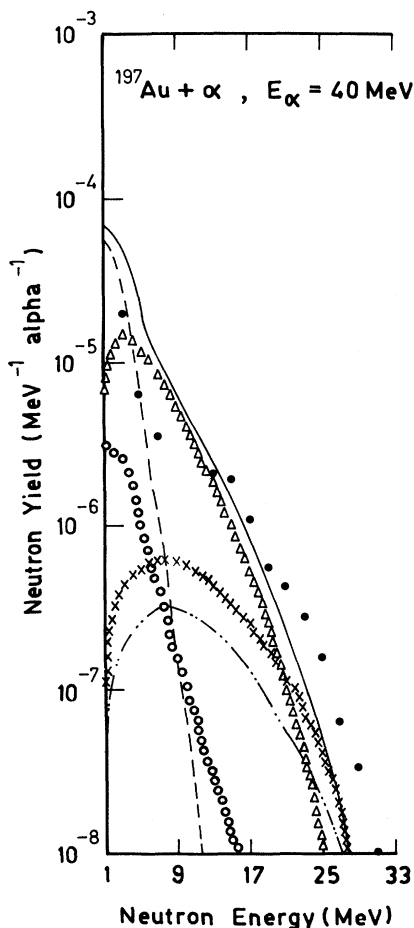

FIG. 9. Same as Fig. 8 for ${}^{197}\text{Au}$ target on 40 MeV incident alpha.

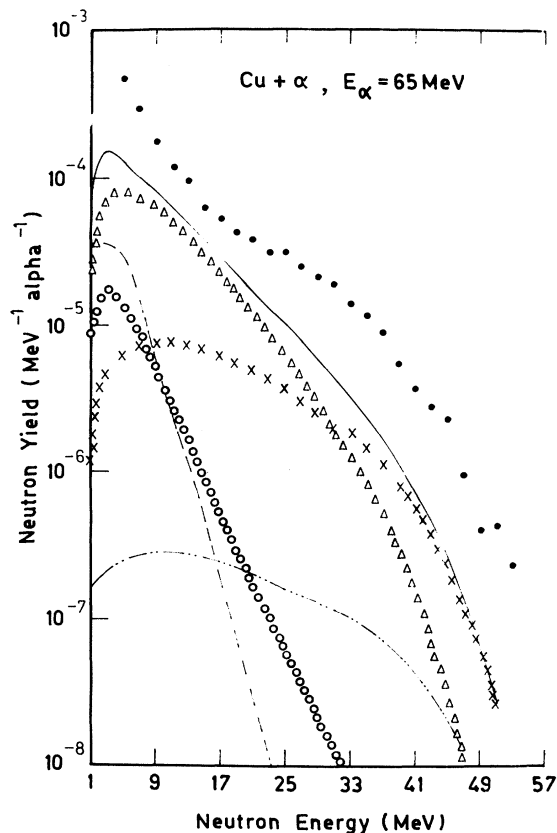FIG. 10. Same as Fig. 8 for Cu target and 65 MeV incident alpha. The experimental points are those of Shin et al. (Ref. 4).
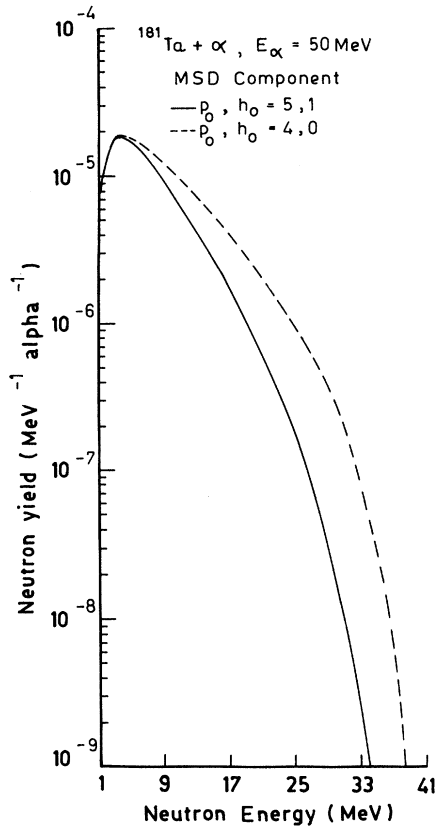
FIG. 11. Comparison of MSD components calculated with the extended exciton model (Ref. 12) for ^{181}Ta and 50 MeV incident alpha for different initial configurations of $p_0, h_0 = 5, 1$ (———) and $p_0, h_0 = 4, 0$ (— — —).

lar distribution of the neutron yield from the same target-projectile combination for the two values of p_0, h_0. The calculated yield with $p_0, h_0 = 4, 0$ shows a significant increase at all angles for energies greater than 9 MeV. The complete dissolution of the alpha, however, is just one of the two processes of its removal from the entrance channel and the absorption of the alpha through the creation of a particle-hole pair is the more likely of the two.[18] It appears from Fig. 12 that admixtures of contributions from initial configurations $p_0, h_0 = 4, 0$ and $p_0, h_0 = 5, 1$ will give better agreement with the observed neutron yield at 30°, 45°, and 90°. But at 0°, even with a 100% contribution from the initial configuration $p_0, h_0 = 4, 0$, the calculated yield remains underpredicted.

In the calculations performed, pairing corrections were not included. To see if inclusion of pairing effects in the excitation energy would correct the discrepancies, both preequilibrium and evaporation component calculations were repeated for ^{181}Ta at 50 MeV incident alpha energy with pairing energies of Gilbert and Cameron.[19] The results for emissions at 0°, where the discrepancy between experiment and calculations is maximum, is shown in Fig. 12. As can be seen, there is no significant change in the neutron spectrum due to pairing corrections.

Another reaction mechanism not considered in the calculations is the breakup of the projectile alpha into binary fragments of ^{3}He and neutron, ^{3}H and proton, and two ^{2}H. One fragment is emitted at forward angles with a velocity corresponding to that of the incident velocity (the Fermi motion of the fragment inside the projectile will cause a spread in the emission velocity). The complementary fragment is absorbed by the target nucleus and the composite system deexcites by preequilibrium and
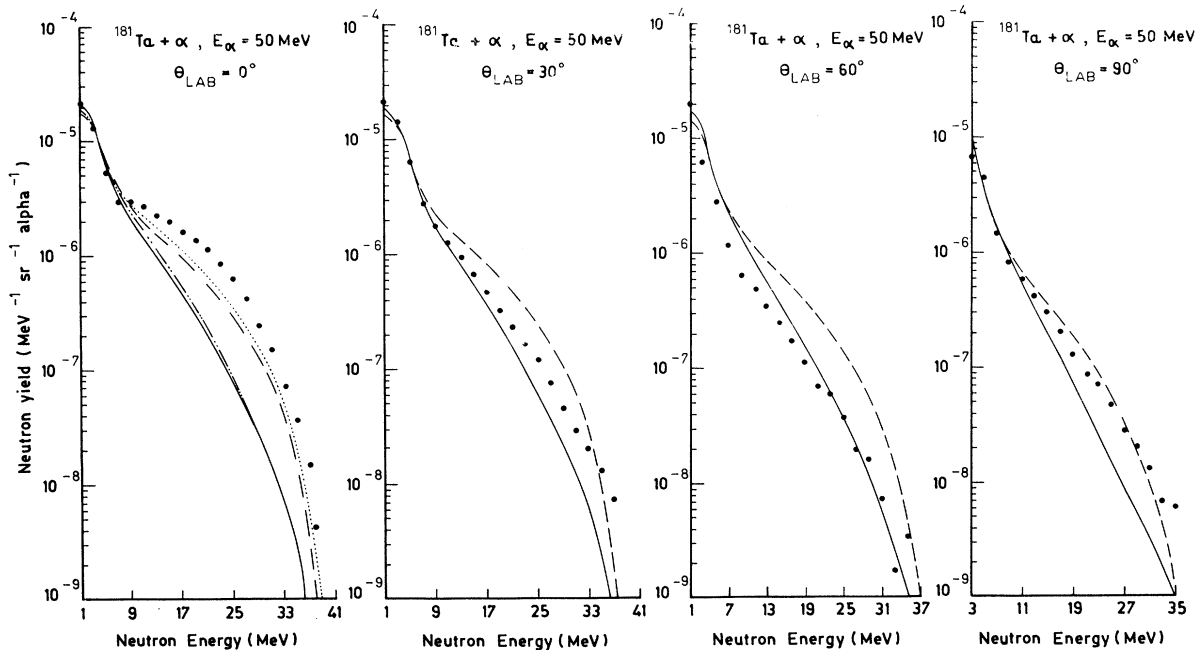

FIG. 12. Comparison of the experimental (●) neutron spectra from ^{181}Ta and 50 MeV incident alpha at 0°, 30°, 60°, and 90° emission angles with calculations of the extended exciton model (Ref 12). The calculations correspond to initial configurations $p_0, h_0 = 5, 1$ (———) and $p_0, h_0 = 4, 0$ (— — —). For $\theta_{lab} = 0°$, calculations with pairing corrections are also shown for $p_0, h_0 = 5, 1$ (— ·· —) and $p_0, h_0 = 4, 0$ (— · — · —).

evaporation emissions. The Q values of (^{3}He,n), (^{3}H,n), and (^{2}H,n) reactions with ^{63}Cu, ^{65}Cu, ^{181}Ta, and ^{197}Au targets are all positive and the high-energy neutron yield will increase due to these reactions. In case the emitted fragment is a neutron, the breakup process will further contribute to the neutron yield around one-fourth of the projectile energy. Inclusion of this mechanism is, however, not going to alter the calculated distributions significantly, since the breakup process constitutes only a small fraction of the total reaction cross section.[18]

IV. CONCLUSIONS

In this paper we have reported the neutron yield obtained from thick targets bombarded by alpha particles. We have tried to understand the reaction mechanisms involved by analyzing our data and some similar data of other workers in terms of the exciton model and compound-nuclear evaporation formalism. The version of the exciton model used includes the contributions from the direct components of nucleon transfer and knockout and MSD and MSC processes. We conclude that the neutron yield from thick targets can be understood in terms of these well-known reaction mechanisms though further investigation of the role played by the direct reaction mechanism is required for a fuller explanation of the data. For this purpose, more experimental data on reaction yields from various target-projectile combinations at different projectile energies are necessary.

ACKNOWLEDGMENTS

[1] T. Nakamura, Y. Uwamino, K. Sato, Y. Furuta, S. Tanaka, S. Ban, H. Hirayama, T. Kosako, K. Kawachi, and Y. Nishihana, At. Data Nucl. Data Tables **32**, 471 (1985).

[2] W. W. Wadman III, Nucl. Sci. Eng. **35**, 220 (1969).

[3] P. H. Stelson and F. K. Mcgowan, Phys. Rev. **133**, B911 (1964); R. L. Macklin and J. H. Gibbons, Nucl. Sci. Eng. **31**, 343 (1968); M. E. Anderson and M. R. Hertz, *ibid.* **44**, 437 (1971); J. K. Bair, *ibid.* **51**, 83 (1973); J. K. Bair and J. Gomez del campo, *ibid.* **71**, 18 (1979); R. A. Cecil, B. D. Anderson, A. R. Baldwin, R. Madey, A. Galonsky, P. Miller, L. Young, and F. M. Waterman, Phys. Rev. C **21**, 2471 (1980).

[4] K. Shin, K. Hibi, M. Fujii, Y. Uwamino, and T. Nakamura, Phys. Rev. C **29**, 1307 (1984).

[5] T. Nakamura, M. Fujii, and K. Shin, Nucl. Sci. Eng. **83**, 444 (1983).

[6] T. Nakamura and Y. Uwamino, Phys. Rev. C **29**, 1317 (1984).

[7] C. Kalbach and F. M. Mann, Phys. Rev. C **23**, 112 (1981); C. Kalbach, *ibid.* **25**, 3197 (1982).

[8] C. A. Fields, F. W. N. De Boer, R. A. Ristenen, P. A. Smith, and E. Sugarbaker, Nucl. Phys. **A377**, 217 (1982).

[9] C. Kalbach, PRECO-D2. Program for calculating preequilibrium and direct reaction double-differential cross sections, Los Alamos National Laboratory Report LA-10248-MS, 1985.

[10] A. Bandyopadhyay, A. Roy, S. K. Dey, S. Bhattacharya, and R. K. Bhowmik, Nucl. Instrum. Methods **204**, 179 (1982).

[11] Y. Uwamino, K. Shin, M. Fujii, and T. Nakamura, Nucl. Instrum. Methods **204**, 179 (1982).

[12] C. Kalbach, Phys. Rev. C **23**, 124 (1984); **24**, 819 (1981).

[13] H. Feshbach, A. Kerman, and S. Koonin, Ann. Phys. (N.Y.) **125**, 429 (1980).

[14] C. Kalbach, Z. Phys. A **283**, 401 (1977).

[15] Y. Iwasaki, Lett. Nuovo Cimento **15**, 439 (1976); Phys. Rev. Lett. **36**, 1464 (1976).

[16] C. F. Williamson, J. P. Boujot, and J. Picard, Centre Etudes Nucleaires de Saclay Report CEA-R3042, 1966.

[17] A. Chatterjee, K. H. N. Murthy, and S. K. Gupta, Pramana **16**, 391 (1981).

[18] E. Gadioli, E. Gadioli-Erba, J. J. Hogan, and B. V. Jacak, Phys. Rev. C **29**, 76 (1984).

[19] A. Gilbert and A. G. W. Cameron, Can. J. Phys. **43**, 1446 (1965).